2024 IEEE/RSJ International Conference on Intelligent Robots and Systems (IROS)
October 14-18, 2024. Abu Dhabi, UAE

Evaluating the Impact of a Semi-Autonomous Interface on Configuration Space Accessibility for Multi-DOF Upper Limb Prostheses

Rebecca J. Greene[1], Christopher Hunt[2], Brooklyn Acosta[3], Zihan Huang[4], Rahul Kaliki[2], and Nitish Thakor[4]

***Abstract*— Powered upper limb prostheses offer a particularly interesting case of human-machine interaction, where the user and the robot are physically coupled as an open chain manipulator. The biological and mechanical degrees of freedom (DOF) must collaborate for the user to manipulate objects in the environment. Current state-of-the-art systems use machine learning models to classify electromyogram (EMG) signals into motion intent primitives, allowing users to move the prosthetic joints sequentially at a fixed velocity. This interface is intended to work for simple systems but does not extend well into higher DOF. Consequently, current commercially available systems are limited to 1 or 2 powered DOF. In this paper, we present a semi-autonomous (SA) hybrid gaze-EMG interface that allows users to command the device in task-space instead of joint-space. Target end-effector poses are selected by tracking the user's gaze vector, and then EMG signals guide the prosthetic along a calculated trajectory towards that pose. To examine how prosthesis interface performance scales with available mechanical DOF, we had 4 subjects complete virtual pick and place tasks with SA and traditional controller interfaces, varying the available DOF in the prosthetic wrist. Our results show that with the SA interface, increased DOF leads to a significant ($p \leq 0.05$) reduction in compensatory motion of the upper arm, more effective ($p \leq 0.01$) utilization of the increased configuration space, and overall more efficient motion ($p \leq 0.01$) than traditional classification based interfaces. These findings indicate that when given SA interfaces, subjects can benefit from fully articulated prosthetic devices, which motivates more clinical research into SA systems and commercial development of higher-DOF devices.**

I. INTRODUCTION

Prosthetic non-wear has been reported in 20% of the adult upper-limb loss population and rejection rates range from 35-40% for myoelectric and cable-controlled systems [1], with 'lack of function' being cited as the main cause of disuse. 88% of upper limb non-prosthetic users claim that the devices are "mentally and physically tiring" to use, while 98% of non-prosthetic users reported being "just as, if not more functional without a prosthesis" [1], [2]. It is important to note that the issues with prosthesis functionality are not due to lack of capability with the mechatronics. Studies in robotic grasping have shown that purely mechanical systems are capable of dexterous object manipulation [3], [4]. The Applied Physics Lab at Johns Hopkins University built a 26DOF upper limb prosthetic to fully emulate the joint motion of a biological limb, but subjects using this device have only utilized at most 3DOF [5]. Commercially available prosthetic devices have at most 2 powered DOF, typically wrist rotation with discrete hand grasps, occasionally with flexion as a 3rd passive joint. There is a substantial difference in dimensionality between the usable configuration space for a prosthesis user's hybrid human-robot serial manipulator and that of a purely biological or robotic arm. This dexterity gap indicates that issues with prosthesis proficiency stem from the human-robot interface and the ability to reliably interpret and execute user intent.

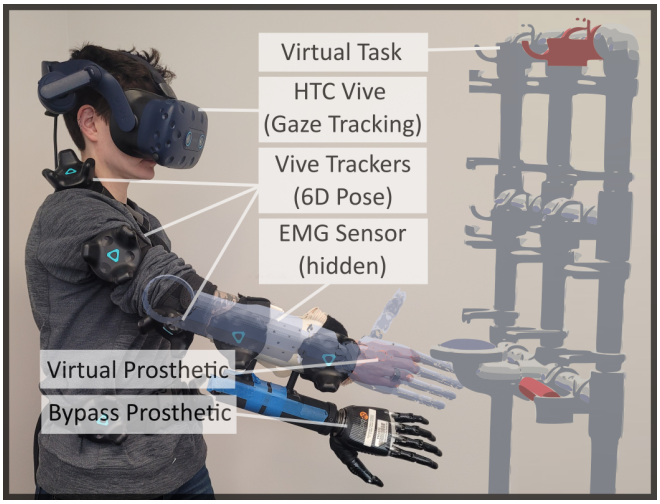

Fig. 1. Illustration of a hybrid gaze-EMG prosthesis interface being used to complete the experimental task. Participants must pick up a red cylinder and transport it to a red holder. The gaze vector can be used to select a target object or holder, and EMG signals can be used to move the prosthetic wrist along a calculated path to align with the target. During the experiment, subjects wore an EMG sensor under a bypass socket for a commercial prosthesis. Although the motion of the physical prosthesis did not directly effect task completion, it was important to consider changes in user behavior due to the inertia. Kinematic trackers were used to measure the motions of the biological limb. Most of the experiment took place in a VR environment rendered by the VIVE headset.

The current paradigm for clinically available powered prosthesis is a feed-forward controller based on classification of motion intent. Electromyogram (EMG) signals are generated by contraction of remaining musculature in the residual limb and can be measured noninvasively by placing elec-

[1]Rebecca J. Greene is with the Department of Electrical and Computer Engineering, Johns Hopkins University, Baltimore, MD, USA rgreen67@jh.edu

[2]Christopher Hunt and Rahul Kaliki are with Infinite Biomedical Technologies Baltimore, MD, USA

[3]Brooklyn Acosta is with the Department of Physics at Dillard University, New Orleans, LA, USA

[4]Zihan Huang and Nitish Thakor are with the Department of Biomedical Engineering, Johns Hopkins University, Baltimore,MD, USA

trodes on the surface of the skin. Today, machine learning-based pattern-recognition (PR) algorithms are considered the state of the art in research [6]. These systems classify EMG signals into a predefined set of motion classes. Pattern-recognition classifiers have seen increasing use in clinical settings [7], although they are still limited in the number of available DOF – typically 1DOF in the wrist (pronation/supination) is combined with a hand that is capable of performing multiple discrete grasps (e.g. 'hand open', 'power', 'tripod', etc). Further, the PR strategy necessitates sequential control of each individual joint. Simultaneous control strategies are being investigated [8], however none have proven sufficiently reliable for clinical use.

Managing even a single prosthetic joint with an EMG-only interface strategy imposes a substantial cognitive burden on the user compared to a biological limb [9]. The extent of this cognitive load increases with the number of extrinsic DOF to be controlled [10]. Even when presented with multiple controllable DOF, subjects using interfaces that require sequential joint modulation tend to utilize just one joint, leading to inefficient and unnatural motion [11], [12]. Ultimately this unnatural compensatory motion leads to long-term overuse injuries, which are a significant health concern that affects many amputees and can lead to a significant decrease in quality of life [1]. Reasons for compensatory motion include lack of joint function in prosthetic devices (especially missing DOF in the wrist) [13], lack of confidence or reliability in the controllable joints that do exist [14], as well as physiological strategies to manage the extra weight of a prosthetic device as compared to a biological limb [15]. These factors, in combination with heavy mental load are cited as the top reasons contributing to prosthesis abandonment [7], [16].

One of the key promises of semi-autonomous systems, especially for the upper limb prosthesis application, is that the controller manages low level joint angle planning while the user retains task-level decision making. Because the biological and mechanical joints are linked serially, traditional approaches to cooperative tasks (like impedance based controllers) are not applicable. Thus the design of appropriate interfaces is a significant and compelling challenge whose outcome has a high impact on the quality of life for patients.

Recently some research groups have begun exploring the use of semi-autonomous prostheses for robust object interaction. Initial iterations in this body of work revolved around the use of camera-based image recognition systems to identify object types and look up appropriate grasp types in response to a 'close' EMG command [17], [18]. Other more empirical approaches have utilized sensorized hands to try to maximize the contact area between the hand and objects for more optimal grasping [19], [20], [21]. In the past 5 years, additional projects have started to include powered wrist rotation as a controllable DOF and would additionally rotate the wrist to maintain user-set wrist angles [23], [24] or the output of a pose recognition system [22], [25]. Semi-autonomous systems exploring wrists with 2DOF have determined wrist angles based on predetermined poses for each recognized object [26] or again to maintain user-set angles [27]. All of these systems use proximity to determine target objects for the semi-autonomous algorithms. This can be an effective method for transradial amputees, who retain enough DOF in the shoulder and elbow to determine palm position, but does not extend well to patients with higher levels of amputation, who arguably have more to gain from semi-autonomous systems. In our previous work, we developed a novel multi-modal interface for a semi-autonomous prosthesis controller, that utilized an estimated gaze vector to determine target objects in a virtual reality (VR) experimental setup, determining grasp type and 1DOF wrist orientation based on object type and pose [28].

In this study, we presented subjects with a refined version of the interface developed in [28] and instructed them to perform a series of pick and place tasks using different prosthetic systems (Fig. 1). Recruited subjects used both Semi-Autonomous (SA) and Pattern Recognition (PR) systems with varying wrist DOF to perform functional tasks in a virtual environment. We evaluated how changes in the available DOF impacted performance metrics related to device functionality and workspace accessibility. This work contributes to the existing literature for semi-autonomous upper limb prostheses in 4 major ways. 1) This is the first semi-autonomous upper limb prosthetic study to consider a 3DOF wrist that fully emulates the functionality of a biological wrist. 2) This is the first semi-autonomous upper limb prosthesis study to examine how variations in the number of controllable DOF impact the user. 3) The results of our study highlight the importance of semi-autonomous systems in high-DOF man-machine systems. 4) Our results show that with semi-autonomous systems, there is now motivation to increase the available powered DOF when building wrists for upper limb prosthesis.

II. SYSTEM DESIGN

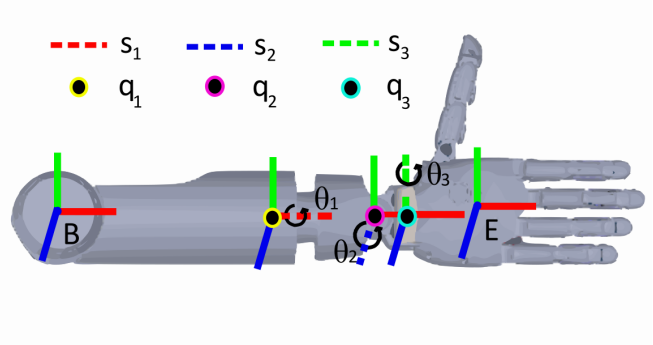

Fig. 2. The transradial virtual modular prosthetic limb (vMPL) can be modeled as a 3DOF wrist with a 1DOF hand. B and E denote the base and palm coordinate frames, respectively. The points q_i and vectors s_i define axes of rotation for each joint. θ_1 rotates the palm around the axis of the forearm, θ_2 sets wrist deviation, and θ_3 corresponds to flexion/extension. A single variable θ_h (not pictured) sets the angle for all 19 finger joints to determine the aperture of the hand.

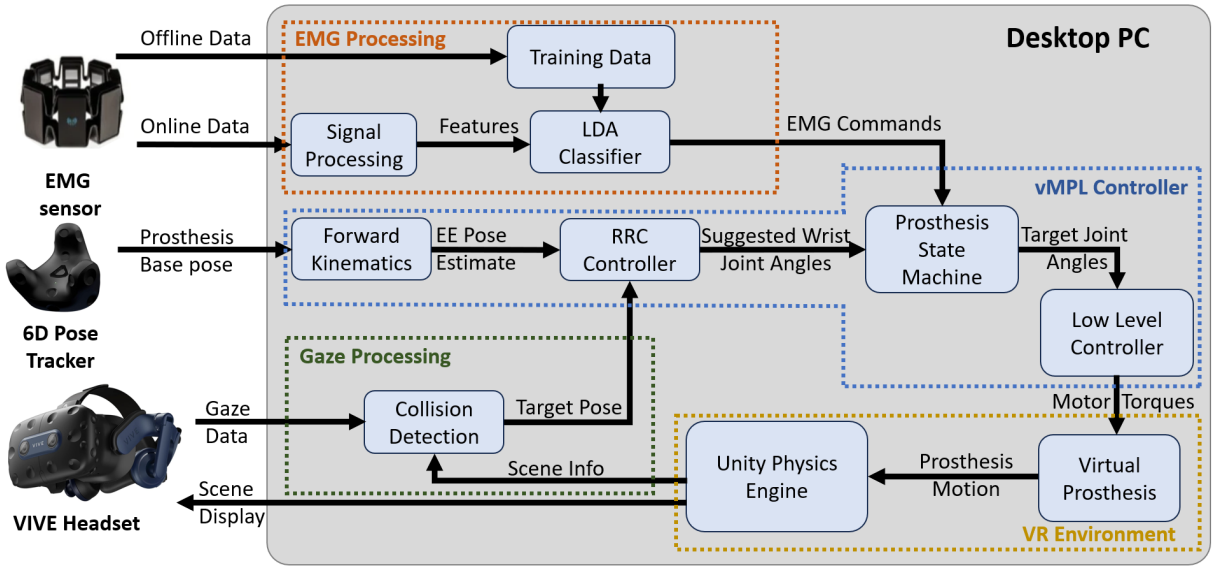

Fig. 3. System diagram for the SA controller. Collisions between gaze vectors sensed from the VIVE headset and features in the VR environment are used to determine the user's desired pose for the prosthetic hand. The location of the base of the prosthetic is determined with a kinematic tracker, and the actual joint angles of the device are used to estimate the current hand pose. Depending on the interface type (PR or SA) and user EMG commands, the target prosthesis joint angles may be those suggested by our algorithm, or come directly from the user.

A. Prosthetic Arm

The vMPL is modelled after the Modular Prosthetic Limb (MPL) from the JHU APL [5]. The MPL is a 26DOF manipulator that includes 3DOF at the shoulder, 1DOF at the elbow, 3DOF at the wrist, and 19DOF in the hand. For use as a transradial prosthetic, we only utilize the lower 22DOF, defining a base at the bottom of the elbow joint (Fig 2). We divide these 22DOF into three wrist joints $\theta_{1:3}$ that define gross motion of the palm, and 19 hand joints θ_h that define the more dexterous configuration of the fingers.

The vMPL and the rest of the Virtual Reality (VR) environment is constructed in Unity 2018 (Unity Software Inc, San Francisco CA, USA) as a series of rigid bodies connected by motor driven hinge joints. Masses for the rigid bodies are set proportionally to the masses of the corresponding parts in the MPL, A low level proportional controller (the 'vMPL arbiter') is used with the vMPL to allow for an abstraction of positional control of $\theta_{1:3}$ and classification control of θ_h. Inputs to the vMPL arbiter consist of target joint angles for the upper arm joints, and a hand class for the lower arm joints. Given a set of target angles, the vMPL controller uses a velocity-limited proportional controller to drive each of the modeled motors:

$$\theta_t = \theta_{t-1} + \frac{K_\theta \Delta_t}{e_{max}} \left(\max(e_{max}, \min(-e_{max}, \theta_t^* - \theta_{t-1})) \right) \quad (1)$$

where t is the timestep, K_θ is the maximum joint angle velocity, Δ_t is the control loop period, e_{max} is a scaling factor, and θ^* is the target angle for the joint.

After using this layer of abstraction, we can now model the vMPL as a 4DOF system with a mobile base (Fig. 2). Using screw theory we can express the pose of the prosthetic palm in the global coordinate frame (g_{st}) as a function of the wrist angles and the pose of the base:

$$g_{st}(\theta_a, t) = g_{sb}(t) e^{\hat{S_1}\theta_1} e^{\hat{S_2}\theta_2} e^{\hat{S_3}\theta_3} g_{bt0} \quad (2)$$

$g_{sb}(t)$ is the transform between the coordinate frame at the base of the prosthesis and the global coordinate frame of the VR system, calculated using kinematic trackers (see Section IV). $\hat{S_1}, \hat{S_2}, \hat{S_3}$ are skew-symmetric matrix representations of the screw axis S_1, S_2, S_3. Each screw axis is a normalized twist, with values v and w corresponding to the linear and angular velocity components respectively.

$$S_i = \begin{bmatrix} w_i \\ v_i \end{bmatrix} = \begin{bmatrix} s_i \\ q_i \times s_i + h_i * s_i \end{bmatrix} \quad (3)$$

Here h_i is the ratio of linear to angular velocity for the twist. Since all of the prosthetic joints are purely rotational, $h_i = 0 \forall i \in [1,3]$. For each joint i, the point q_i and vector s_i define the axis of rotation as shown in Fig. 2.

B. Hardware

Although the experimental task was completed with a virtual prosthetic, subjects were outfitted with a commercial prosthetic system to to account for changes in behavior due to the device weight. This setup included a bebionic3 prosthetic hand (Ottobock, Duderstadt, Germany) and Motion Control Wrist Rotator (Fillauer LLC, Chattanooga, TN), mounted on a bypass socket that allowed the non-amputee subjects to mount the prosthesis on their forearm. EMG data was acquired using a Myo Armband EMG sensor (Thalmic Labs, Ontario, CA).

To render the VR environment, the system uses the VIVE Pro Eye head-mounted display (HMD) (HTC Corporation, New Taipei City, Taiwan) (Fig. 1). The HMD also contains

internal eye-tracking hardware that allows the system to measure visuomotor behavior such as gaze direction and visual attention (Tobii Technology AB, Stockholm, Sweden). HTC VIVE trackers (HTC Corporation, New Taipei City, Taiwan) were mounted on both hips as well as the shoulder, upper arm, elbow, forearm, and wrist of a participant's dominant limb to record the trunk and arm kinematics. 6D pose information was sampled from each tracker at 90 Hz. When calculating outcome metrics 3D position data was filtered in both the forward and backwards directions using a 6-Hz second-order Butterworth low-pass filter [29]. Orientation data was filtered using spherical linear interpolation of the pose quaternions [30]. The forearm tracker was also used to superimpose the virtual prosthetic on top of the user's limb for the experimental task.

C. EMG Classification

The eight bipolar electrodes on the EMG sensor were sampled at 200 Hz. No digital signal filtering was necessary due to front-end EMG signal conditioning incorporated into the armband [31]. For each EMG channel, five time-domain signals [32] (mean absolute value, variance, waveform length, zero crossings, and slope sign change) were extracted from 250 ms windows, with a 50 ms step between windows, as is standard in the literature [33]. This led to a total of 40 features per time window. At the beginning of each experimental session, subjects trained a Linear Discriminant Analysis (LDA) classifier to translate EMG signals into commands to the prosthesis.

The LDA algorithm calculates a new set of basis vectors for the labeled dataset, chosen to minimize within-class scatter σ_W^2 while maximizing inter-class scatter σ_B^2 within the training data.

$$\sigma_W^2 = \sum_{c=1}^{C} \sum_{i=1}^{N_c} (x_{ci} - \mu_c)(x_{ci} - \mu_c)^T \tag{4}$$

$$\sigma_B^2 = \sum_{c=1}^{C} N_c (\mu_c - \mu)(\mu_c - \mu)^T \tag{5}$$

Where $x_{ci} \in \mathbb{R}^{\#feat \times 1}$ is a datapoint belonging to class c, given C total classes each with N_c datapoints, class means μ_c, and training set mean μ.

Once the new basis vectors are calculated, each new datapoint x is rebased and classified according to its maximum a posteriori probability, assuming a Gaussian distribution for each class:

$$c_{\text{pred}} = \underset{c}{\operatorname{argmax}} \, (x - \mu_c)^T \Sigma_c^{-1} (x - \mu_c) \tag{6}$$

Training data for the classifier was taken in 9 separate arm positions spanning the expected 3D workspace for the experiment. Subjects were presented with visual and verbal cues for different classes in each arm position and instructed to hold each class for 2 seconds per position.

An additional majority vote post-processing filter was added at the output of the classifier.

$$c_{\text{out}} = \text{mode}\big(c_{\text{pred}}(t - L : t)\big) \tag{7}$$

The filter length L was varied on a per-session basis during classifier training. Higher values of L improved output stability but reduced responsiveness. Experimental values of L ranged from 10-35 windows (0.5s - 1.75s) and were set as the lowest possible value that still achieved noise-free class transitions.

D. Pattern Recognition User Interface

When using the PR interface, motion of the prosthetic joints corresponded directly to the output of the EMG classifier c_{out} (See Eq. 8). For the 1DOF system, subjects trained a classifier to differentiate between 5 different classes: 'Rest', 'Hand Close', 'Hand Open', 'Pronate', and 'Supinate'. A 'Rest' class would maintain the current prosthesis configuration. A 'Hand Close' or 'Hand Open' command would direct the vMPL arbiter to move the hand into the specified grasp. 'Pronate' and 'Supinate' classes increase or decrease θ_1 at a fixed rate according to Eq. 8. For the 2DOF system, subjects added two additional EMG classes to control θ_2, 'Flexion' and 'Extension'. At 3DOF 'Abduction' and 'Adduction' were added to control θ_3. See Fig 4 for images of the corresponding wrist classes and motions.

$$\theta_i(t+1) = \theta_i(t) + \text{sign}(c_{\text{out}}) K_q \tag{8}$$

where i is the wrist joint indicated by c_{out}, and K_q is an angular velocity set by the subject according to preference during training. The function $\text{sign}(c_{\text{out}})$ designates the direction of motion a particular class will exert on a joint (e.g. 'Pronate' decreases θ_1, while 'Supinate' increases it)

E. Semi-Autonomous User Interface

With the Semi-Autonomous interface, subjects utilize a combination of gaze direction and EMG classifier output c_{out} to command the joint angles of the vMPL. Information about the pose of the selected object is used to calculate optimal palm orientation. Because this experiment takes place in a virtual environment, all information about the environment is easily accessible to the controller. These idealized conditions allow us to analyze the impact of the user interface independent of pose estimation system accuracy.

When designing the interface, we took care to ensure that the prosthetic joints will never move without direct input from the user. If the user disagrees with the calculated wrist motion, they are able to assume manual control of the prosthesis. Additionally, if no target pose has been selected, the interface will remain in manual mode. When in manual mode, the device responds identically to the PR interface, where the motion of the prosthesis is a direct reflection of the c_{out} class predicted by the EMG classifier. If there is no direct user activity in manual mode for more than 2s, the interface will switch back to SA Mode (Fig. 4).

When no object is making contact with the palm, gaze can be used to select a target object from the environment, and the palm pose g_{se}^* is set to the object pose. When there is contact to the palm, placement locations can be selected from a predefined subset, and g_{se}^* is set to the pose associated with the selected location. A red box is drawn on the VR

display to indicate the selected object or placement location. A visual cursor on the VR display indicates the estimated gaze vector and the calculated controller motion.

Once a target pose has been selected, the default mode for the interface is SA Mode. Target poses g^* are indicated with the gaze vector. During training, the user selects one of the available wrist classes (e.g. 'Pronate") to designate as a wrist cue c_{cue}. The original function of c_{cue} is replaced, and it is instead used to drive the prosthesis along a controller calculated path towards the target pose. Use of any of the other EMG wrist classes will switch the interface to Manual Mode, and then the corresponding action will be performed.

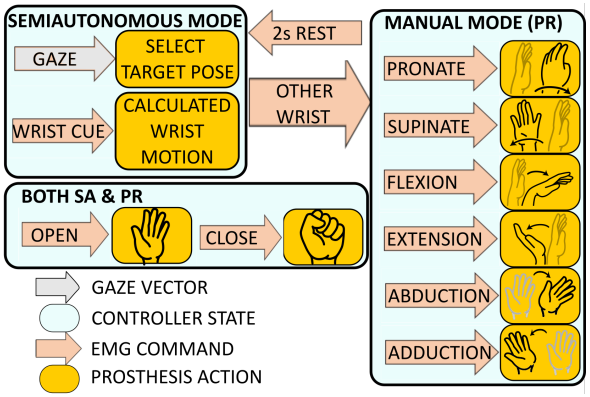

Fig. 4. The workflow of the user interface with the SA controller. A 'Rest' class will maintain the current prosthetic configuration. A 'Hand Open' command will always open the hand, and a 'Hand Close' command will always close the hand. Subjects select one wrist command to cue calculated wrist rotation that will align the prosthesis palm with the target pose. Other wrist commands will put users into a 'manual mode' where prosthesis motion corresponds directly to EMG commands (as in the PR interface). A sustained 'Rest' command will return the user to 'shared' mode.

F. Trajectory Planning

When users generate the c_{cue} EMG class in Semi-Autonomous Mode, a Resolved Rate Controller (RRC) algorithm is used to drive the available prosthetic wrist joints towards g^*_{se}. The velocity of the wrist motion is proportional to the pose error expressed in twist coordinates ξ:

$$q_{t+1} = q_t - K_q \Delta_t J_b^{-1} A \xi \tag{9}$$

where K_q is a constant determined by the subject, Δ_t is the period of the control loop, A is a weighting matrix selected to emphasize the rotational component of the pose error, and J_b is the body Jacobian relating the velocities of the controllable DOF to the end-effector twist. The ith column of J_b can be calculated as:

$$J_{bi}(\theta) = \mathrm{Ad}_{e^{S_n\theta_n}\ldots e^{S_{i+1}\theta_{i+1}}} S_i \tag{10}$$

where S_i is as defined in Eq. 3, and Ad_g denotes the adjoint representation of a rigid body transformation matrix $g = (R, p) \in SE(3)$. This is used to change the reference of a twist motion or wrench force, between two frames related by g.

$$Ad_g = \begin{vmatrix} R & 0 \\ [p]R & R \end{vmatrix} \in \mathbb{R}^{6x6} \tag{11}$$

$$[p] = \begin{vmatrix} 0 & -p_3 & p_2 \\ p_3 & 0 & -p_1 \\ -p_2 & p_1 & 0 \end{vmatrix} \tag{12}$$

III. EXPERIMENTAL PROCEDURE

Participating subjects were asked to perform a pick-and-place task in a VR environment (Fig. 1), using either a SA or a PR controller. A total of 4 non-amputee subjects were recruited (1 female, 3 male), aged 23-29. Subjects had no known neurological disorders and varying levels of experience with myoelectric pattern recognition algorithms. All subjects had prior experience with VR platforms, and two had a known proclivity to VR-induced motion sickness. All subjects were right-handed. Informed consent was obtained from all subjects, and the study was conducted with the approval of the Johns Hopkins Medical Institutional Review Board.

During the experiment, the vMPL was superimposed on top of a subject's biological limb using a kinematic tracker. Subjects then utilized the vMPL to manipulate virtual objects in the experimental task. Subjects were presented with a total of 6 different prosthesis systems, varying both the number of available DOF in the wrist (1-3) and the interface type (PR or SA). Wrist DOF were added in an order to reflect their importance in performing Acts of Daily Living [13].

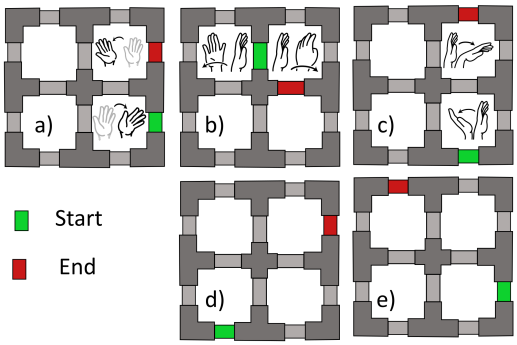

Fig. 5. Subjects were presented with 5 types of pick and place task, each repeated 10 times in a randomized order. Three of the task types (a,b,c) were designed to encourage single-DOF activations of the wrist. Two of the tasks (d,e) were designed to elicit multi-DOF wrist activations.

A. Experimental Task

To evaluate the various system designs, subjects performed a pick and place task on a virtual Prosthetic Hand Assessment Measure (vPHAM) [34]. The vPHAM system comprises an adjustable windowpane structure, with six horizontal and six vertical segments, each outfitted with an object holder (Fig 5). The experimental task consisted of 5 different variations of pick and place task, each repeated 10 times in a randomized order. Three of the task types were designed to encourage single-DOF activations of the

wrist. Two of the tasks were designed to encourage multi-DOF wrist activations. A button is also included in the frame to enable user-driven timer control. Pressing the button starts/stops a timer that is used to determine completion time for each manipulation. Physical and virtual versions of the PHAM have been used in studies of upper limb motion with non-amputee and amputee subjects, using transradial and transhumeral prostheses [34].

B. Experimental Protocol

The experimental protocol followed an AB single case experimental design (SCED). Each of the recruited subjects used the SA and PR systems interchangeably for a minimum of six training sessions and six testing sessions over a period of 4-6 weeks. For Sessions A_n, participants operated PR systems, while for Sessions B_n, participants operated SA systems. Subjects trained on all 6 systems at least once in order of increasing DOF before beginning any testing sessions. Both PR and SA systems were presented to each subject the same number of times for any DOF to prevent biases from the learning effect. Half of the subjects were presented with the SA system first while the other half was presented with the PR system first, to prevent biases in user preference.

In any given session, subjects began by calibrating the EMG classifier and the gaze tracker . If the subject was able to achieve reliable EMG class access (determined if all class-wise true positive predictions were $\geq 95\%, \geq 90\%, \geq 85\%$, for the 1-, 2-, and 3DOF systems respectively) and had already trained on each interface/DOF combination at least once, then the session could qualify as a testing session. On both training and testing sessions, subjects spent up to 15 minutes in a sandbox environment of randomly generated tasks. During this time they were able to make modifications to the wrist rotation speed K_q, c_{cue} selection, and recalibrate the classifier or gaze tracker if desired. Each task type was repeated $10\times$, for a total of 50 tasks presented in a randomized order. Throughout the tasks, subjects were instructed to keep their feet planted to reduce trunk motion, ensuring that most compensatory motion was restricted to the upper arm.

IV. RESULTS & DISCUSSION

A. Completion Rate

A given task was considered successful if subjects placed the object in the correct holder within a 15s time limit without dropping it. The small sample size of our dataset (4 subjects) limits the statistical significance of cumulative metrics. Trends in the data show that with the SA system task completion rate increased with the available DOF. The PR interface showed the opposite trend, with completion rates decreasing as wrist DOF were added (Fig 6). It is worth noting that the distribution of completion times for successful tasks remained relatively fixed over controller types and available DOF. This means that the increased efficiency of motion in the SA controller made up for any delays incurred by adding an extra process step of target pose selection.

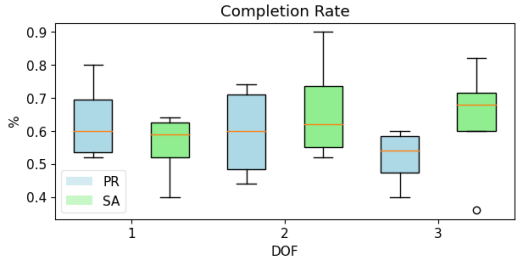

Fig. 6. Task completion rates were evaluated for both interfaces types as the available prosthetic DOF was increased. Even with a limited sample size we see a trend towards increased completion rates with increased DOF when using a SA controller, but a decrease in completion rates with increased DOF with the PR controller.

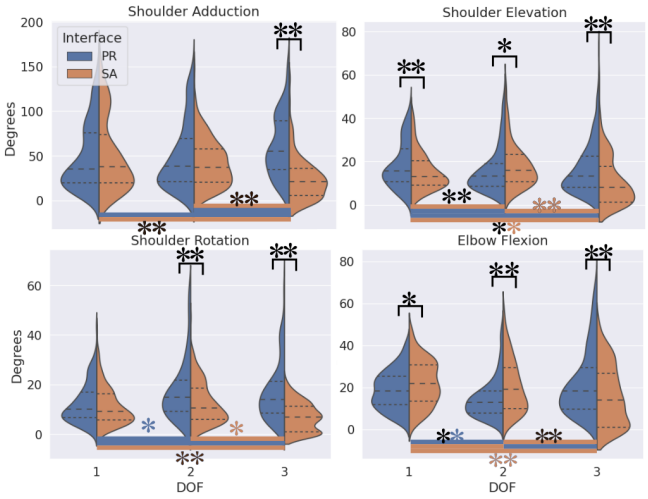

Fig. 7. For each successfully completed task we show the range of motion ($\theta_{max} - \theta_{min}$) for the joints in the upper arm. A lower range of motion, especially in more proximal joints, indicates increased biomechanical efficiency. $*$ and $**$ denote statistical significance ($p \leq 0.05$) and ($p \leq 0.01$). A black color indicates that the significance holds for both PR and SA systems, while blue/orange denote significance for that respective system.

B. Compensatory Motion

Because the arm is a 7DOF system (even more DOF if we consider the motion of the torso) performing a 5DOF task, there is sufficient redundancy in the shoulder to overcome errors in palm orientation after wrist motion. However, due to the decreased lever arm, it is generally more biomechanically efficient for orientation changes to take place in the more distal joints (e.g. wrist), rather than at the shoulder or torso. Thus an important measure of prosthesis performance is the amount of compensatory motion that occurs in the residual limb. In prior work the amount of compensatory motion has typically been determined by considering the range of motion for each biological joint, with a lower value signifying less compensation [11]. We calculated the shoulder elevation angle as the angle in the saggital plane between the vector of the upper arm and the vector of the torso. We defined shoulder abduction as the angle of the upper arm in the transverse plane relative to the torso. Humeral rotation was calculated as rotation around the axis of the upper arm, and elbow flexion was computed as the angle between the upper

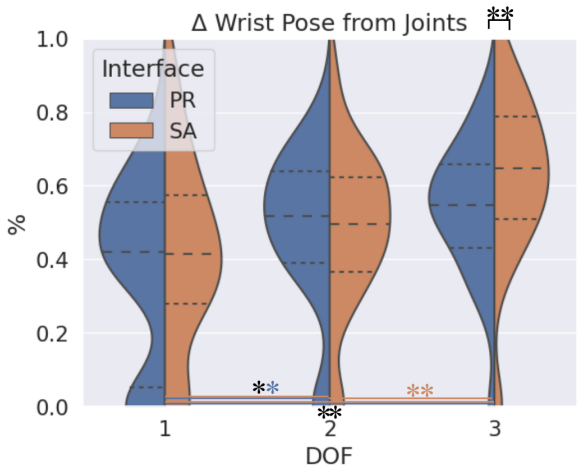

Fig. 8. For every successfully completed task, we calculated the ratio of pose changes in the wrist due to prosthetic joint motion against the total number of pose changes.

arm and the lower arm.

Our results (Fig 7) show that with the SA controller there was a decrease in compensatory motion in the shoulder as we increased the DOF of the system ($p \leq 0.01$). Statistical significance was calculated with a Wilcoxon rank-sum statistic. There was a similiar decrease in compensatory shoulder adduction for the PR system from between 1 and 2 DOF. But when a third PR DOF was added, compensatory motion in shoulder elevation and rotation ($p \leq 0.001$) was worse than with less articulated systems. There was significantly less shoulder motion ($p \leq 0.05$) with the 3DOF SA system than the 3DOF PR system. At 2 and 3DOF there was an increase in the range of motion in the elbow of the SA systems as compared to the PR systems, but we believe this to be a positive finding, as it is more biomechanically efficient for the motion to take place in the elbow rather than the shoulder.

Additionally, we examined what percentage of the wrist pose changes were due to motion in the wrist joints, as opposed to motion in more proximal parts of the kinematic chain (Fig 8). The count for wrist pose changes considered instances where the difference in global rotation quaternion between frames had a norm above a noise threshold of $\varepsilon = 0.005$. When increasing the available DOF from 1 to 2 there was a statistically significant increase in the amount of rotation due to the wrist joints for both interfaces ($p \leq 0.05$). For the SA interface, there was a further increase from 2 to 3DOF ($p \leq 10^{-6}$), but no significant change for the PR interface.

C. Path Efficiency

Illustrative sample trajectories for some of the different task types are show in Fig 9. Simply by offering simultaneous joint motion, the SA controller results in more efficient motion through joint angle space, and less overall wrist joint motion ($p \leq 0.01$) for all DOF cases. Further, the percentage of inexpedient wrist motion (that actually increased pose error) was significantly lower with the SA controller as

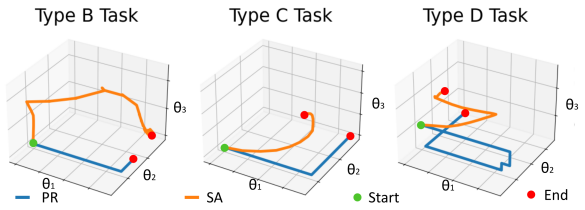

Fig. 9. Sample paths through joint angle space for different task types with both the 3DOF SA and PR controller. Start locations are marked with green, end locations in red. Because the PR interface necessitates sequential motion, it is inherently less efficient than the SA controller.

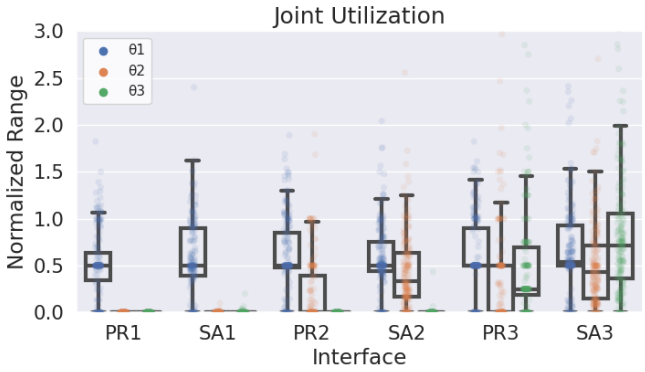

Fig. 10. For all successful trials, the path length for each joint angle is normalized to the overall range of motion for that joint. Normalized path length for each trial are plotted as points with with low opacity, and a boxplot summarizes the distribution. Even when provided more DOF, users with the PR interface will largely rely on a single joint.

compared to the PR controller at 2 and 3DOF ($p \leq 0.05$).

To assess the accessibility of the configuration space, we considered the utilization of the available joints for each controller configuration. For all successful trials we measured path lengths for each joint independently, and then normalized by the range of motion for the joint (Fig. 10). Using the SA controller, there is notably more utilization of the extra configuration space when subjects are given 2 and 3DOF ($p \leq 10^{-4}$). With the PR interface, the median joint path length for θ_2 is 0 degrees for all DOF configurations. Further, for the PR interfaces, path lengths cluster at multiples of the joint angle range. This indicates that users would simply activate a joint until hitting the range of motion limit. In the SA controller we see a more even spread of values, implying better graded proportional control.

V. CONCLUSION

This study examines the impact of expanded DOF for patients using robotic upper limb prostheses and the importance of using semi-autonomous interfaces to make those DOF accessible. The experiment took place in a virtual environment due to the lack of availability of multi-DOF prosthetic wrists. We present a hybrid gaze-EMG user interface for a controller that allows users to plan in task-space instead of joint-angle space. Our results show a substantial ($p \leq 0.001$) reduction in compensatory motion with each added DOF when using the SA controller, while PR users stop benefiting after 2DOF.

Combined with our analysis of configuration space paths, we see that PR users tend to rely on a single prosthetic joint, preferring biomechanically inefficient and damaging compensatory motion in the trunk and upper arm. Our trends show performance improvement as we increase DOF with a SA controller and decreased or saturated performance with the PR controller. This study considered the transradial case, but when extrapolating to higher levels of amputation (transhumeral, shoulder disarticulation), the value of a semi-autonomous system only becomes more significant.

A notable limitation of this study is that our subject pool consists entirely of people with intact limbs. Individuals with intact limbs typically exhibit superior performance with EMG-classification systems compared to persons with some degree of upper limb loss. Thus we expect that the performance gap between the PR and SA controllers would only grow with a more targeted subject population. Now that we have verified the value of fully articulated wrists and semi-autonomous interfaces, future work in this area includes transitioning to a physical testing platform and recruitment of a more clinically relevant subject pool. Additionally, examination of bio-mimetic or other trajectory planning methods is an open problem, especially for systems that include an elbow or shoulder joint, which play a more significant role in palm placement as well as orientation.

ACKNOWLEDGMENT

We thank Peter Kazanzides and Noah Cowan for advice and comments on the manuscript.

REFERENCES

[1] Østlie K, et al. Mental health and satisfaction with life among upper limb amputees: a Norwegian population-based survey comparing adult acquired major upper limb amputees with a control group. Disabil Rehabil. 2011;33(17-18):1594-607.

[2] Biddiss EA, Chau TT. Upper limb prosthesis use and abandonment: a survey of the last 25 years. Prosthet Orthot Int. 2007 Sep;31(3):236-57.

[3] F. J. Chu,et al. "Real-World Multiobject, Multigrasp Detection," in IEEE Robot Autom Let, vol. 3, no. 4, pp. 3355-3362, Oct. 2018

[4] F. Song, et al. "Learning Optimal Grasping Posture of Multi-Fingered Dexterous Hands for Unknown Objects," 2018 IEEE Int Conf ROBIO, Kuala Lumpur, Malaysia, 2018, pp. 2310-2315

[5] Yu, K.E. et al. "Clinical evaluation of the revolutionizing prosthetics modular prosthetic limb system for upper extremity amputees," Sci Rep 11, 954 (2021).

[6] M. Simão et al. "A Review on Electromyography Decoding and Pattern Recognition for Human-Machine Interaction," in IEEE Access, vol. 7, pp. 39564-39582, 2019,

[7] Resnik, L. et al. Evaluation of EMG pattern recognition for upper limb prosthesis control: a case study in comparison with direct myoelectric control. J NeuroEng Rehabil 15, 23 (2018).

[8] Y. Gloumakov et al. "Trajectory Control–An Effective Strategy for Controlling Multi-DOF Upper Limb Prosthetic Devices", in IEEE Trans Neural Syst Rehabil Eng, vol 30. pp. 420-430, 2022.

[9] R. Rackerby et al. "Understanding and Measuring the Cognitive Load of Amputees for Rehabilitation and Prosthesis Development," Archives of Rehabilitation Research and Clinical Translation, vol. 4, no. 3, p. 100216, Sep. 2022.

[10] J. Lafo et al. "Cognitive Characteristics Associated With Device Adoption, Skill Retention, and Early Withdrawal From a Study of an Advanced Upper Limb Prosthesis," Am J Phys Med Rehabil, vol. 98, no. 10, pp. 879–887, Oct. 2019.

[11] M. Legrand et al., "Simultaneous Control of 2DOF Upper-Limb Prosthesis With Body Compensations-Based Control: A Multiple Cases Study," in IEEE Trans Neural Syst Rehabil Eng, vol. 30, pp. 1745-1754, 2022

[12] M. J. Major et al. "Comparison of range-of-motion and variability in upper body movements between transradial prosthesis users and able-bodied controls when executing goal-oriented tasks," J NeuroEng Rehabil, vol. 11, no. 1, p. 132, 2014.

[13] M. Deijs, et al. "Flexible and static wrist units in upper limb prosthesis users: functionality scores, user satisfaction and compensatory movements," J NeuroEng Rehabil, vol. 13, no. 1, p. 26, Dec. 2016.

[14] J. Davidson, "A survey of the satisfaction of upper limb amputees with their prostheses, their lifestyles, and their abilities," Journal of Hand Therapy, vol. 15, no. 1, pp. 62–70, Jan. 2002.

[15] A. Valevicius et al. "Compensatory strategies of body-powered prosthesis users reveal primary reliance on trunk motion and relation to skill level," Clinical Biomechanics, vol. 72, pp. 122–129, Feb. 2020.

[16] L. C. Smail et al. "Comfort and function remain key factors in upper limb prosthetic abandonment: findings of a scoping review," Disability and Rehabilitation: Assistive Technology, vol. 16, no. 8, pp. 821–830, Nov. 2021.

[17] S. Došen et al. "Cognitive vision system for control of dexterous prosthetic hands: Experimental evaluation," J NeuroEng Rehabil, vol. 7, no. 1, p. 42, Dec. 2010.

[18] M. Markovic et al. "Stereovision and augmented reality for closed-loop control of grasping in hand prostheses," J. Neural Eng., vol. 11, no. 4, p. 046001, Aug. 2014.

[19] K. Z. Zhuang et al., "Shared human–robot proportional control of a dexterous myoelectric prosthesis," Nat Mach Intell, vol. 1, no. 9, pp. 400–411, Sep. 2019.

[20] T. C. Hansen et al. "A Bionic Hand for Semi-Autonomous Fragile Object Manipulation via Proximity and Pressure Sensors," in 2021 43rd Int Conf EMBC, Mexico: IEEE, Nov. 2021, pp. 6465–6469.

[21] N. Thomas et al. "Haptic shared control improves neural efficiency during myoelectric prosthesis use," Sci Rep, vol. 13, no. 1, p. 484, Jan. 2023.

[22] B. Zhong et al. "Reliable Vision-Based Grasping Target Recognition for Upper Limb Prostheses," IEEE Trans. Cybern., vol. 52, no. 3, pp. 1750–1762, Mar. 2022.

[23] D. A. Bennett et al. "IMU-Based Wrist Rotation Control of a Transradial Myoelectric Prosthesis," IEEE Trans. Neural Syst. Rehabil. Eng., vol. 26, no. 2, pp. 419–427, Feb. 2018.

[24] J. Starke et al. "Semi-autonomous control of prosthetic hands based on multimodal sensing, human grasp demonstration and user intention," Robot Autonom Syst, vol. 154, p. 104123, Aug. 2022.

[25] M. N. Castro and S. Dosen, "Continuous Semi-autonomous Prosthesis Control Using a Depth Sensor on the Hand," Front. Neurorobot., vol. 16, p. 814973, Mar. 2022.

[26] J. Mouchoux et al. "Artificial Perception and Semiautonomous Control in Myoelectric Hand Prostheses Increases Performance and Decreases Effort," IEEE Trans. Robot., vol. 37, no. 4, pp. 1298–1312, Aug. 2021.

[27] N. Seppich et al., "CyberLimb: a novel robotic prosthesis concept with shared and intuitive control," J NeuroEng Rehabil, vol. 19, no. 1, p. 41, Dec. 2022.

[28] R. J. Greene et al. "Shared Control of Upper Limb Prosthesis for Improved Robustness and Usability," 2022 9th IEEE RAS/EMBS Int Conf BioRob, Seoul, Korea, Republic of, 2022, pp. 1-7,

[29] M. A. Murphy, et al. "Kinematic variables quantifying upper-extremity performance after stroke during reaching and drinking from a glass," Neurorehabilitation and neural repair, vol. 25, no. 1, pp. 71–80, 2011.

[30] Shoemake, Ken. "Animating Rotation with Quaternion Curves." ACM SIGGRAPH Computer Graphics Vol. 19, Issue 3, 1985, pp. 245–254.

[31] Pizzolato, Stefano et al. "Comparison of six electromyography acquisition setups on hand movement classification tasks," PLOS ONE, vol. 12 no. 10, 2017.

[32] Hudgins, B. et al. "A new strategy for multifunction myoelectric control," IEEE Trans. Bio-Med. Eng. vol. 40, p.82-94, 1993.

[33] Smith, Lauren H.et al. "Determining the optimal window length for pattern recognition-based myoelectric control: Balancing the competing effects of classification error and Controller Delay," IEEE Trans. Neural Syst. Rehabil. Eng., vol. 19 no. 2, p. 1866-192 2011.

[34] C. Hunt et al. "PHAM: Prosthetic Hand Assessment Measure" in: Proceedings of MEC17, Myoelectric Controls Symposium. Fredericton, NB, Canada, 14-19. August 2011